Assessing Utilization Boundaries for Pt-Based Catalysts in an Operating Proton-Exchange Membrane Fuel Cell

Michal Ronovsky, Lujin Pan, Malte Klingenhof, Isaac Martens, Raphael Chattot, Lukas Fusek, Peter Kus, Marta Mirolo, Fabio Dionigi, Harriet Burdett, et al.

Assessing Utilization Boundaries for Pt-based Catalysts in an Operating PEMFC

Michal Ronovsky[1], Lujin Pan[2], Malte Klingenhof[2], Isaac Martens[1], Raphael Chattot[1], Lukas Fusek[3], Peter Kus[3], Marta Mirolo[1], Fabio Dionigi[2], Harriet Burdett[4], Jonathan Sharman[4], Peter Strasser[2], Alex Martinez Bonastre[4], Jakub Drnec[1]

[1] ESRF—The European Synchrotron, ID 31 Beamline, Grenoble, France
[2] Electrochemical Energy, Catalysis and Material Science Laboratory, Department of Chemistry, Technical University Berlin, Berlin, Germany
[3] Charles University, Faculty of Mathematics and Physics, Department of Surface and Plasma Science, V Holešovičkách 2, 180 00, Prague 8, Czech Republic
[4] Johnson Matthey Technology Centre, Blount's Court, Sonning Common, Reading RG4 9NH, U.K.

Abstract

Octahedra (oh) PtNiX catalysts have attracted attention due to their exceptional catalytic activities toward the oxygen reduction reaction in proton-exchange membrane fuel cells (PEMFCs). Here, we investigate the degradation dynamics of oh-PtNiIr in fuel cell conditions by operando X-ray Diffraction. Two XRD-coupled square-wave accelerated stress tests (0.6 to 0.95) V and (0.7 to 0.95) V confirm that dissolution and overall degradation strongly depend on the lower potential limit, as already observed in previous works for PtCo catalysts. By directly observing the extent of oxidation during potential cycling, we link the alloy redox dynamics to the stability. The studied catalysts' stability is proportional to both the extent of oxidation and, more interestingly, the degree of reduction. Comparing a benchmark Pt catalyst with oh-PtNiIr allows for associating the differences between oxidation and reduction potentials and the optimal usage window for each class of catalysts. This simple method can be employed to find the operation boundaries of the PEMFC to minimize the degradation of a large class of Pt-based catalysts, without time-consuming stress tests.

Introduction

As we try to reduce our carbon footprint, a hydrogen economy is becoming integral to transitioning to a carbon-neutral future. Given the critical role of noble metals for Oxygen Reduction Reaction (ORR) catalysis, much research has been dedicated to improving the catalytic activity of Pt by modifying the electronic and structural properties via Pt alloying with transition metals (Co, Ni, Fe, Ir) (Marković et al. 2001), (Asset et al. 2018), (Kim et al. 2019), (Gasteiger et al. 2005), (C. Zhang et al. 2017), (Sharma and Andersen 2018), (Lin et al. 2020). In 2007, Stamenkovic et al. identified the most active surface: Pt3Ni(111), which led to the development of PtNi octahedra NPs with 10-fold activity gain due to maximizing the surface of (111) facets (Stamenkovic et al. 2007), (Cui et al. 2012). However, transferring the activity measured in rotating disc electrode (RDE) experiments to PEMFC and reaching stability targets remains a significant challenge (Pan et al. 2019).

Several factors play the role. Octahedra (oh) NPs (5-8 nm) have a smaller electrochemical surface area (ECSA) than commercial 2-3 nm Pt catalysts. Thus, octahedra must accommodate and withstand a larger current per nanoparticle. Accommodating increased current density (per nanoparticle) requires a well-structured boundary that allows sufficient oxygen diffusion as well as proton and electron conductivity (Ly, Asset, and Atanassov 2020), (O'Hayre and Prinz 2004), (Kongkanand and Mathias 2016). Further, withstanding potential changes during PEMFC operation is the biggest challenge because the dissolution of nickel or platinum degrades the finely-tuned structure and thus lowers the catalytic

activity. One way to stabilize the structure is to dope oh-PtNi with a small amount of additional metal such as Ir, Mo, or Rh (Dionigi et al. 2019), (Li et al. 2018). While this is a promising improvement, and the stability objectives are reached in the RDE configuration, the stability still does not satisfy the target when tested in the MEA configuration following the DOE testing protocol.
For another class of ORR catalysts, PtCo intermetallics and benchmark Pt catalysts, it has been observed that a stress test's potential limits and potential cycling protocol greatly impact the overall stability (Gatalo et al. 2022), (Ahluwalia et al. 2018), (Myers et al. 2018). Faster scan rates generally lead to less dissolution; thus, square-wave test profiles mimic more realistic catalyst usage (Kneer et al. 2018). It has been hypothesized that this is linked to the Pt redox dynamics, where the oxidation extent of surface Pt atoms leads to various degrees of dissolution and degradation. To this extent, much research has focused on the Pt oxidation-dissolution link. Many publications highlighted the influence of upper potential limit (UPL) in an accelerated stress test, making clear that increasing the UPL increases the extent of oxidation and, in turn, the extent of dissolution (Cherevko et al. 2015), (Topalov et al. 2014), (Huang et al. 2014), (Imai et al. 2009), (Myers et al. 2018), (Drnec et al. 2017), (Ruge et al. 2017b), (Wang, Kumar, and Myers 2006), (Fuchs et al. 2020). However, only a limited amount of research focused on the influence of lower potential limit (LPL) (H. Zhang et al. 2013), (Uchimura et al. 2008). In the most recent work, Đukić et al. pointed out the importance of controlling LPL to improve the PEMFC catalyst's lifetime, which is somewhat linked to the reduction process (Đukić et al. 2022). Nevertheless, the actual mechanism between LPL and the stability of the catalyst in the MEA remains an open question.

Here we look at the dissolution mechanics of a PtNiIr/C octahedra catalyst (doped with <1 at. % of Ir) and compare it with a reference Pt/C catalyst. With a focus on LPL, we investigate the linkage between the catalyst degradation and operational boundaries in 5 cm^2 PEMFC optimized for high-energy X-ray diffraction (XRD) measurement. The fast acquisition rate enabled by the EBS-ESRF allows tracking oxidation/reduction processes during the PEMFC operation with a high temporal resolution. Moreover, the determination of potential onsets of oxidation and reduction and their relation to the observed degradation is presented. We conclude that Pt and Ni dissolution is proportional not only to the extent of Pt oxidation but, interestingly, also to the extent of Pt reduction. Limiting LPL is possible if the longevity of the catalyst layer is a concern. However, such an approach greatly limits the maximum power density obtainable from the PEMFC.

Results and discussion

For the experiments shown in this work, we use the catalyst-coated membranes (CCMs) of two types: (i) "Pt(JM)" benchmark CCM with Pt (volume weighted diameter is 2.9 nm as determined using XRD) on both cathode (0.187 mg_{Pt}/cm^2) and anode (0.079 mg_{Pt}/cm^2) that serves as reference material; (ii) "oh-PtNiIr" CCM (volume weighted diameter is 7.1 nm) with PtNiIr (0.100 mg_{Pt}/cm^2 and 0.017 mg_{Ni}/cm^2) at the cathode and Pt at the anode (0.079 mg_{Pt}/cm^2). See the experimental section for more details. Interestingly, we find that the oh-PtNiIr catalyst incorporated in the CCM already has a different composition from the as-synthesized oh-PtNiIr powder: EDX analysis shows that the oh-PtNiIr powder has an atomic Pt:Ni ratio of 2.20, whereas the as-prepared oh-PtNiIr CCM has the ratio of 6.35. This suggests that the catalyst lost 57% of its Ni content during the ink-making and printing. Such a high loss of transition metal alloying element has been observed and discussed previously in the work of (Gatalo et al. 2022), (Dubau et al. 2015). It has been pointed out that the CCM-making process, together with the activation potential cycling, alters the catalyst morphology and composition to such an extent that the catalyst is no more the same material as synthesized, questioning the common approaches to catalyst activity testing using the RDE technique (Chattot et al. 2022). Our results provide further evidence that this is also the case for multimetallic oh-PtNiIr. In contrast to compositional changes, the structural changes are less noticeable in the ink-making/printing step (Figure 1a,b). Qualitatively, the edges of octahedral nanoparticles are less pronounced in the catalyst coated on the membrane than in the catalyst powder. Figure 1c shows the catalyst after 10k

cycles of a standard (0.6 to 0.95) V accelerated stress test (AST). At the end of life (EOL), the atomic Pt:Ni ratio is 8.33, meaning an additional 21% of Ni content leaches out. Thus, almost three times more Ni content dissolved during the ink-making/printing procedure compared to the AST. It is clear that to retain the composition of state-of-the-art multimetallic catalysts during the MEA preparation, serious attention must be focused on adapting the ink-making/printing procedure.
From Figure 1c, we can see that Ni dissolution itself is not the only degradation mechanism. Nanoparticles also aggregate, coalesce, ripen, and carbon support corrodes (Cherevko 2018), (Prokop, Drakselova, and Bouzek 2020), (J. Zhang et al. 2021), (Okonkwo et al. 2021). In the following section, we perform a series of ASTs discussing the effects of lower potential boundaries on catalyst degradation.

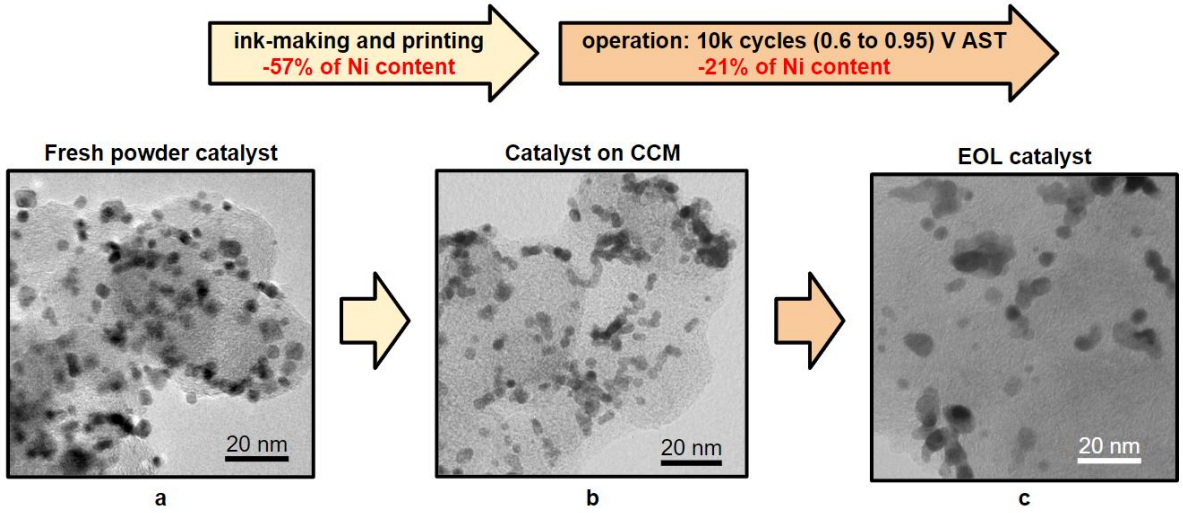

Figure 1: Transmission electron microscopy images of oh-PtNiIr catalyst at three stages: a) as-prepared powder, b) as-prepared CCM, and c) end-of-life catalyst after 10k cycles of (0.6 to 0.95) V AST. The ink-making/printing procedure leached out 58% of Ni content and made the edges of octahedra less pronounced. The AST leached out only 23% of Ni content but caused severe structural degradation.

Accelerated stress tests

In laboratory conditions, catalyst degradation is studied by square-wave accelerated stress tests. U.S. DRIVE Fuel Cell Technical Team adopted the standard of cycling from (0.6 to 0.95) V with a 3 s dwell time at both lower potential limit and upper potential limit. This test mimics the dynamics of the typical FC operation with Pt dissolution and Ostwald ripening as preferential degradation pathway (Sasaki, Shao, and Adzic 2009), (Topalov et al. 2014), (Cherevko et al. 2015), (Sandbeck et al. 2020), (Ehelebe et al. 2021). Even though the mechanism of Pt degradation and dissolution as a function of upper potential limit is well known (Lopes et al. 2018), (Khedekar et al. 2021), (Bi, Gray, and Fuller 2007), (H. Zhang et al. 2013), (Martens, Chattot, and Drnec 2022)(Martens2019), the exact nature of the rather surprising linkage between LPL and Pt degradation is still unclear (Gatalo et al. 2022)(H. Zhang et al. 2013)), (Đukić et al. 2022), (Gatalo et al. 2022), (Uchimura et al. 2008).

In order to study the effect of lower potentials on the aging of oh-PtNiIr and Pt(JM) catalysts, we perform two ASTs with different LPLs (0.6 to 0.95 V and 0.7 to 0.95 V). We use a custom-built 5 cm^2 fuel cell operating at 80 °C, at 80% relative humidity, flowing H2/N2 at 200 sccm to mimic the conditions of commercial devices (Martens, Vamvakeros, et al. 2019), (Martens et al. 2021). Both Pt(JM) and oh-PtNiIr MEAs made from as-prepared CCMs with Sigracet 22BB GDLs were conditioned at 500 mA/cm^2 for approximately two hours. Throughout the 10k cycles of each AST, we follow structural changes of the catalyst with XRD (Martens, Vamvakeros, et al. 2019). In general, we track four XRD parameters: scale factor, microstrain, lattice parameter, and crystallite size.

1. Scale factor, i.e. scattering intensity, corresponds to the total amount of scatterers. Martens et al. proposed that scale factor decreases at oxidation potentials due to the formation of an amorphous oxide layer on Pt NPs (Martens, Chattot, et al. 2019). The scale factor is thus a direct indicator of the amorphous oxide growth/reduction onset.

2. Microstrain originates from local defects in the lattice (Leineweber 2011; Chattot et al. 2018). Such defects can be generated by various surface processes and through diffusion distributed in the bulk of the NP, giving rise to the broadening of the diffraction peaks (Chattot et al. 2018) (Kawaguchi et al. 2021). One mechanism causing the microstrain increase is a place exchange, where the structural defects are formed during the extraction of Pt atom (Drnec et al. 2017) (Fuchs et al. 2020) (Ruge et al. 2017a) (Jacobse, Rost, and Koper 2019), (You et al. 1994), (Nagy and You 2002), (You and Nagy 1994). Another possibility is the dissolution of less noble metal from alloyed NPs, where the process leaves the defects throughout the bulk of nanoparticles. (Kongkanand and Ziegelbauer 2012).
3. Lattice parameter is a global measure of strain. In bimetallic systems, the changes can be caused by dissolution, following Vegard's law (Vegard 1921) (Denton and Ashcroft 1991), or by the evolution of surface tension due to the field effect and adsorption phenomena (Weissmüller et al. 2003) (Chattot et al. 2021).
4. Crystallite size is the size of the coherently scattering domain. The size of the scattering domain does not change during aggregation, but it is the degradation process of coalescence and ripening when the size of the scattering domain changes. Thus, depending on the degradation process, one nanoparticle can be composed of a few such domains (Martens, Chattot, and Drnec 2022). Harsher degradation leads in general to a more pronounced crystallite size increase.

Figure 2 shows the evolution of crystallite sizes of Pt(JM) and oh-PtNiIr and lattice parameter of oh-PtNiIr throughout 10k cycles. As expected, the 0.6 V LPL AST is harsher as the crystallite size of the NPs increases throughout 10k cycles by 42% for Pt(JM) and 30% for oh-PtNiIr, whereas in the case of the 0.7 V LPL AST by only 17% for Pt(JM), and 10% for oh-PtNiIr. The degradation and ripening of NPs are the fastest at the beginning of the AST for both catalysts. In Figure 2b, we show the evolution of the lattice parameter of the oh-PtNiIr catalyst for 0.6 V LPL AST (stars) and 0.7 V LPL AST (diamonds). Nickel dissolution is more substantial in the case of 0.6 V LPL AST as the lattice parameter increases by 0.4%, corresponding to an 18% loss of Ni at atomic percent, which is in line with the 21% loss of Ni at atomic percent measured by EDX. In contrast, in the case of the 0.7 V LPL AST, Ni loss was only 4% at atomic percent. Similar to the size increase, Ni dissolution is also the fastest at the beginning of the AST. These observations agree with the previously reported dependency of dissolution on LPL for Pt (H. Zhang et al. 2013) and Pt-alloyed nanocatalysts (Gatalo et al. 2022).

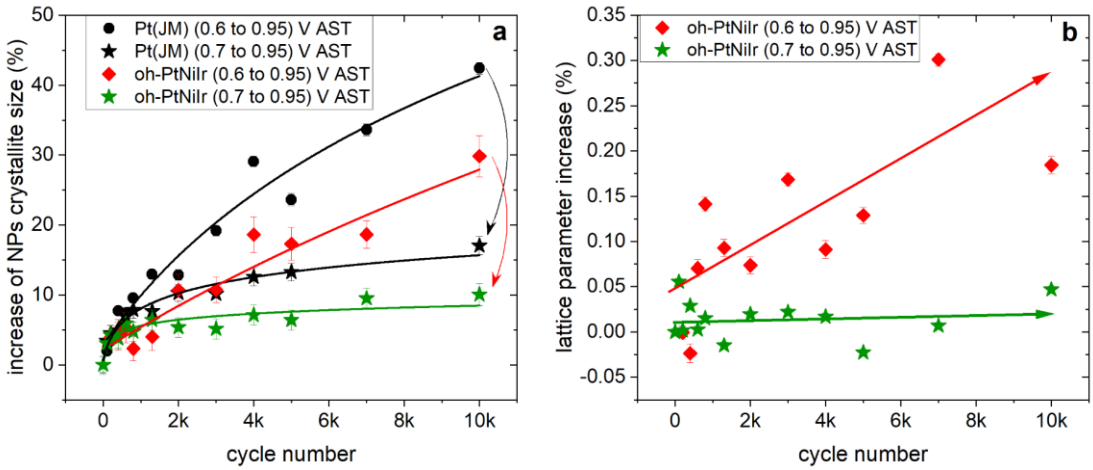

Figure 2: a) crystallite size evolution of Pt(JM) (black) and oh-PtNiIr (red/green) catalysts during 10k cycles of two ASTs. In the case of (0.6 to 0.95) V AST, Pt(JM) size increase is 42% and for oh-PtNiIr 30%, whereas in the case of (0.7 to 0.95) V AST, Pt(JM) size increase is 17% and for oh-PtNiIr 10%. b) lattice parameter evolution of oh-PtNiIr for (0.6 to 0.95) V and (0.7 to 0.95) V AST.

X-ray diffraction coupled with cyclic voltammetry

To build the connection between the LPL and dissolution mechanism, we follow the cyclic voltammetry with XRD in the course of several cycles (XRD-CV). CV measures current density which originates from overlaying non-faradaic and faradaic processes. Coupling with XRD, we further distinguish contributions from adsorption and place-exchange-induced oxidation as the first is measured by changes in lattice parameter and the latter by a decrease in scale factor. The top part of Figure 3 shows the evolution of scale factor (brown) and microstrain (green) during CV (blue) (50 mV/s) for Pt(JM). The bottom part shows the same for oh-PtNiIr. As the first CV cycle is clearly different from the subsequent ones due to impurity removal and reconstruction of the surface, only the second cycle is shown (Chattot et al. 2022). (For more information about the measurement protocol, see the experimental section in supporting information.)

To ambiguously follow the growth of surface oxide, we start the anodic sweep at 0.05 V where the catalyst is fully reduced. In general, the XRD scale factor follows the oxidation hysteresis apparent in CV. It is constant up to the onset of the oxidation potential, after which it decreases until the reverse potential of 1.23 V. At the beginning of the cathodic sweep, the scale factor rests at its lowest value and starts increasing when the potential crosses the onset of the reduction potential. After passing a reduction region (highlighted in red), the scale factor returns close to its original value. There is a slight slope between the end of the reduction region and 0.05 V in the cathodic sweep, pointing to the fact that the catalyst is not yet entirely reduced. A small number of catalytic sites, presumably highly oxophilic defects, are much harder to reduce giving rise to this slope (Janik, McCrum, and Koper 2018), (Chattot et al. 2020). Nevertheless, the reduction is ~97% complete at the end of the reduction region. Further, there is a slight difference between both oxidation and reduction onsets for Pt(JM), but no difference is observed for oh-PtNiIr within our 0.02V resolution limit.
In agreement with the CV profiles, the reduction region is shifted towards higher potentials for the oh-PtNiIr compared to the Pt(JM) catalyst. This is a consequence of OH bond weakening, which is related to a d-band shift induced by alloying with less noble metal (Hammer and Nørskov 2000), (J. K. Nørskov et al. 2009), (Jens K. Nørskov et al. 2011), (Kitchin et al. 2004), (Xin et al. 2014). Clearly, a d-band shift not only enhances ORR activity but also shifts the oxidation onset to higher potentials, defining the stability window of the catalyst (Drnec et al. 2017). This is then expressed by lesser oxidation during AST and, therefore, slower degradation and higher stability of PtNi catalysts overall (Figure 2a).

Next, we turn to the general trend of microstrain, distinguishing between the formation of amorphous surface oxide and other processes causing the increase of general disorder of atoms within the NPs. Such processes can be triggered by a place exchange during the oxidation onset, in which the localized surface strain caused by Pt-O swap, or dealloying where defects formed due to the Ni dissolution, inhomogeneously propagates to the bulk of the particle (Kawaguchi et al. 2021). Microstrain follows a similar trend as the scale factor: it is constant in the (0.3 to 0.9) V range and then increases until sweep reversal. Upon reversal, it holds its value, and after the 0.9 V is crossed, it starts to decrease again until it reaches a plateau at 0.6 V. No difference between anodic and cathodic microstrain onsets is observed. An additional feature is present in the range of (0.05 to 0.3) V, where microstrain drops to its lowest value at 0.05 V. This part is associated with the HUPD region, in which adsorbed hydrogen likely further anneals the surface and, subsequently, the bulk of NPs, leaving behind a fully reduced, well-ordered catalyst without structural impurities in the lattice.

For Pt(JM), microstrain onset is at higher potentials than scattering intensity onset. This is due to the fact that a sufficient amount of amorphous oxide must be present on the surface before the surface microstrain propagates to the bulk and is therefore detectable by X-ray measurement. For oh-PtNiIr, microstrain increases in the anodic scan even before the formation of the amorphous oxide. This might be due to the preferential oxidation of Ni

atoms (A. Politano et al. 2013), (Antonio Politano and Chiarello 2016), with the suggested formation of subsurface Ni-O species (Lee et al. 2016), leaving behind structural defects even before the Pt-O place exchange kicks in. Additionally, it is likely that only a small amount of Ni-O species is necessary to trigger defect propagation into the bulk as the oh-PtNiIr catalyst has intrinsically higher microstrain due to alloying. The potential window of microstrain decrease in the cathodic scan is shorter, suggesting that the relaxation processes are faster for oh-PtNiIr. Considering that the Ni-O bond is weaker than Pt-O (A. Politano et al. 2013), faster overall kinetics likely translates to faster Ni-O reduction (and dissolution) compared to Pt-O. Consequently, oh-PtNiIr alloy pays the price for better kinetics by higher sensitivity to secondary metal leaching while cycling.

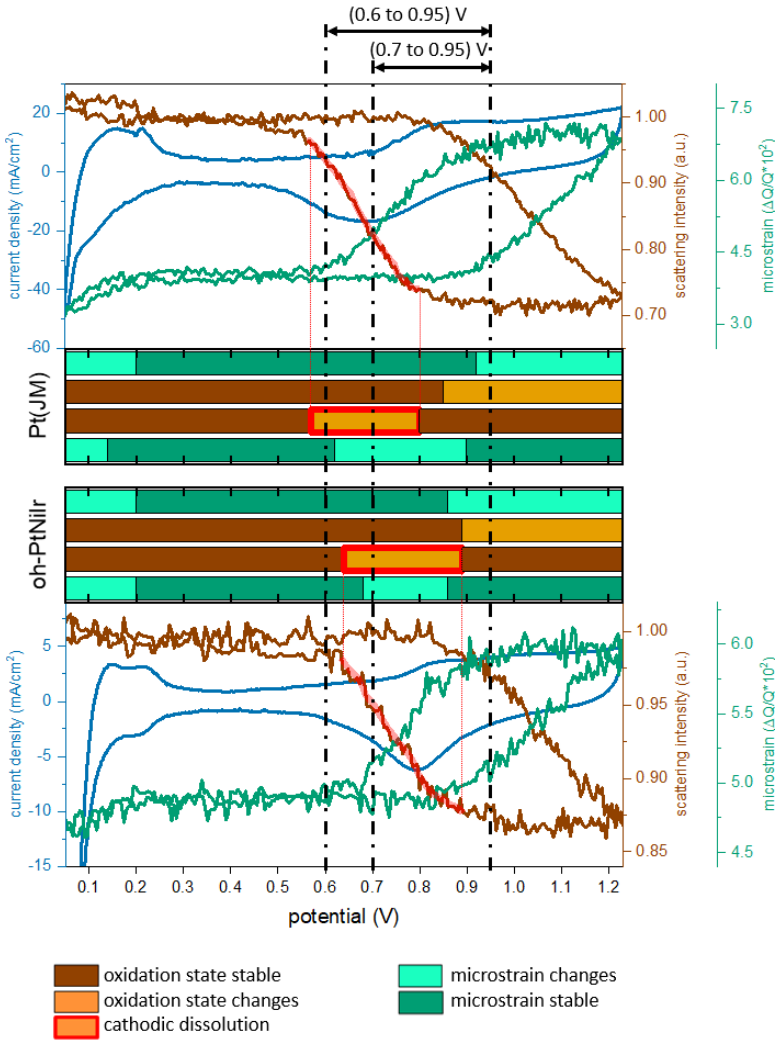

Figure 3. X-ray diffraction coupled with cyclic voltammetry. Scale factor (brown) and microstrain (green) were obtained with XRD during (0.05 to 1.23) V CV with a 50 mV/s scan rate. The upper half corresponds to the Pt(JM) and the lower part to the oh-PtNiIr. An increase in defect concentration during oxidation increases the microstrain value. The catalyst's oxidation is accompanied by a reversible decrease in scattering intensity. In the raw data, the cathodic dissolution region is highlighted by a red curve that extends into a simplified diagram where the dissolution region is highlighted by a red box. Black vertical dash-dot lines mark the potential boundaries of two types of ASTs to connect XRD-CV with long-term stability.

Finally, we connect the degradation data from ASTs with the oxidation/reduction dynamics deduced from XRD-CV. First, oh-PtNiIr does not oxidize to such a large extent at UPL as Pt(JM), giving the of-PtNiIr catalyst better overall stability. Second, the 0.6 V LPL results in a fully reduced oh-PtNiIr catalyst, while at 0.7 V LPL, the reduction is only partial for both Pt(JM) and oh-PtNiIr. Given that the reduction region is where the most dissolution happens, the dissolution amount must be proportional to both the degree of oxidation and the degree of reduction, and this is clearly shown by the XRD-CV measurement. This result also implies that the most oxophilic sites which are more difficult to reduce, likely the least coordinated

sites, are also prone the most to dissolution. Therefore, one of the strategies to limit the dissolution is to keep those vulnerable sites permanently oxidized.

Such knowledge has a direct implication for the operation of a fuel cell, especially involving high-active shape-controlled platinum alloys. Their activity is strongly bound to a specific crystal structure, and the extent of surface restructuring during the reduction will affect this activity to a larger extent than other catalysts. In general, if we want to preserve high performance, we must carefully select the operational boundaries and limit both the lower and higher potential boundaries regardless of the catalyst type. Moreover, in the automotive industry, where multimetallic catalysts will be used to lower the stack's cost, the loss in power density at higher LPL can be compensated by an increased exchange current density of a more active catalyst and its higher electric efficiency.

Conclusion

We have shown the practicality of the XRD-CV technique to explain the degradation behavior and provided further important insight into catalyst degradation mechanisms in the operational PEMFC. We have found specific onsets of key crystallographic parameters (microstrain and scale) associated with the oxidation, reduction, and degradation for two types of catalysts. For oh-PtNiIr, platinum oxidation and reduction are shifted towards higher potentials compared to the Pt(JM) catalyst due to the d-band shift, and subsequent weakening of the OH bond, induced by alloying with a less noble metal. By employing two AST with different lower potential limits (0.6 to 0.95) V and (0.7 to 0.95) V, we confirm the dependence of catalyst degradation on the lower potential limit.
By combining these two results, we conclude that the extent of degradation is proportional not only to the degree of oxidation but also to the degree of reduction within a cycle, independently of the catalyst's nature. In order to preserve the crystalline structure of oh-PtNiIr and thus its high catalytic activity, an operational boundary has to be set on both lower and higher potential limits. This approach will work best for automotive applications where a multimetallic catalyst reduces the stack's price and its increased exchange current density with higher electric efficiency do not reduce the power density. We think that limiting LPL is a crucial step for implementing alloyed catalysts into PEMFCs and FC automotive as such. Moreover, the presented simple and fast methodology can be further developed to serve as a benchmark measurement to explore the operation boundaries for all kinds of Pt-based catalysts.

Providing Potential Reviewer Names

Please suggest at least four recommended reviewers for the manuscript. Include the address and email address for each suggested reviewer. Authors may request certain individuals not be used as reviewers. Authors are encouraged to avoid suggesting reviewers from the authors' institutions. Do not suggest reviewers who may have a real or perceived conflict of interest. Whenever possible, suggest academic email addresses rather than personal email addresses.

Supporting Information

Experimental

Catalyst powders

Johnson Matthey supplied carbon-supported Pt nanoparticles with average sizes of 2.9 nm as determined by XRD. The oh-PtNiIr catalyst powder was prepared on Vulcan XC72R by a seed-mediated solvothermal method (manuscript in preparation). Two batches of ~500 mg

each were prepared. The atomic composition of each batched analyzed with ICP-OS yielded $Pt_{68.2}Ni_{31.2}Ir_{0.5}$ and $Pt_{68.3}Ni_{31.3}Ir_{0.4}$ with Pt wt% of 30.1 and 29.0, respectively. For the first batch, TEM measurements showed a number-weighted nanoparticle size of (3.8 +- 1.6) nm. For the second batch, two particle sizes were identified. Bigger nanoparticles had the number-weighted NP size (4.5 +- 1.7) nm, and smaller nanoparticles were (2.7 +- 1.7) nm in size. The volume-weighted nanoparticle size determined by XRD was 5.9 nm. A slightly larger volume-weighted NP size is a sign of non-symmetrical size distribution with the tail towards larger NPs, which is in line with TEM of the second batch. Batches were mixed to make the ink for CCMs.

Membrane electrode assemblies

CCMs printed from the catalyst powders were supplied by Johnson Matthey. For both types of CCMs, the anode is carbon-supported Pt with 0.079 mg_{Pt}/cm^2 loading. MEAs were prepared by cutting the CCM into 5 cm^2 pieces and aligning SGL 22BB GDL on both sides. For Pt(JM), the cathode loading is 0.187 mg_{Pt}/cm^2 with the average nanoparticle size determined by XRD of 2.9 nm. For oh-PtNiIr, the cathode loading was 0.100 mg_{Pt}/cm^2, 0.017 mg_{Ni}/cm^2, with the average nanoparticle size determined by XRD of 7.1 nm. In this case, quantitative single-nanoparticle size distribution analysis with TEM would not give a reasonable value as NPs formed chains of several crystallites, as seen in Figure 1b.

Fuel cell and operation protocol

As-prepared MEAs were used in a custom fuel cell described in previous literature (Martens, Vamvakeros, et al. 2019). The cell was operated at 80 °C, with 80% relative humidity on the anode and cathode. MEAs for the AST experiments were conditioned at constant current density for (1 to 3) h: oh-PtNiIr 0.6 V LPL @ 140 mA/cm^2; 0.7 V LPL @ 400 mA/cm^2; Pt(JM) 0.6 V LPL @ 500 mA/cm^2; 0.7 V LPL @ 500 mA/cm^2. MEAs for the XRD-CV experiments were conditioned at 0.6 V for approximately 2 h (Figure S1). In this case, constant potential conditioning was chosen to limit dissolution by oxidation and reduction. For both types of conditioning and the ASTs, the gas flow was 200/100 sccm O_2/H_2 with an additional 0.5 bar backpressure. For XRD-CV, the gas flow was 100/100 sccm N_2/H_2 with an additional 0.01 bar backpressure.

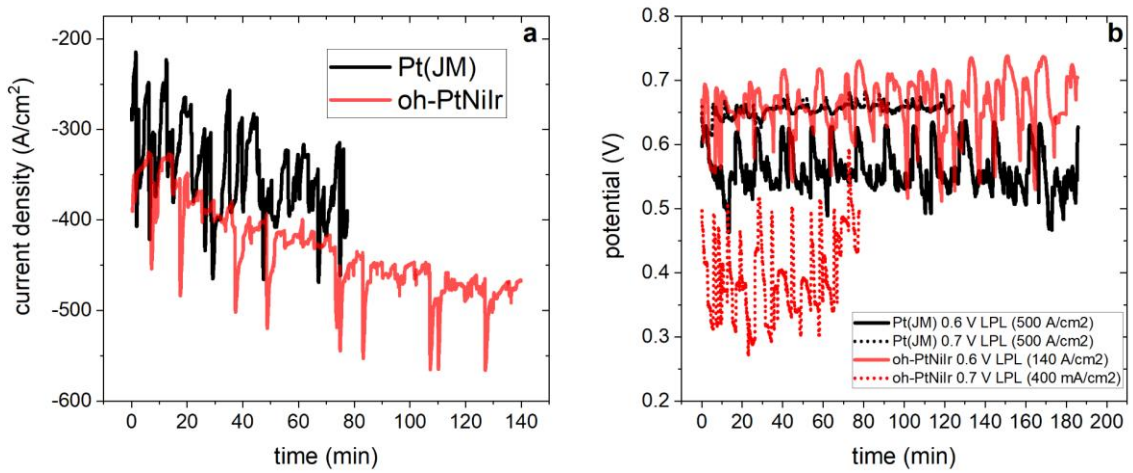

Figure S1: a) MEA conditioning of Pt(JM) and oh-PtNiIr MEA at 0.6 V for XRD-CV experiments. b) MEA conditioning for two types of ASTs 0.6 V LPL and 0.7 V LPL.

Electrochemistry

SP240 Biologic potentiostat was connected in the 4 electrodes setup. Voltage cables were connected directly to graphite flow fields, and the current was collected from the adjacent copper blocks (Martens, Vamvakeros, et al. 2019). Cyclic voltammetry was performed from 0.05 V to 1.23 V at 50 mV/s, flowing N_2/H_2 300/200 sccm at 80 °C, with 80% relative humidity. The protocol starts at 0.47 V, after compensation for ohmic drop at 85% amplitude. The first scan from 0.47 V to 1.23 V and back to 0.05 V is referred to as the 1st cycle. The second cycle shown in the Results and Discussion chapter starts at 0.05 V. Figure S2 shows the first two cycles for Pt(JM). We see that during the first cycle (dashed line) the catalyst

oxidizes at higher potentials than in the subsequent cycle. This is due to impurity desorption from an overall restructuring of the surface (Chattot et al. 2022). These impurities have to be removed by oxidation and reduction during the first cycle to get a clean surface that represents the actual catalytic properties of the catalyst. It shows the importance of reporting at least the second cycle to obtain relevant electrochemical information. In our experiments, subsequent cycles had the same characteristics as the second cycle.

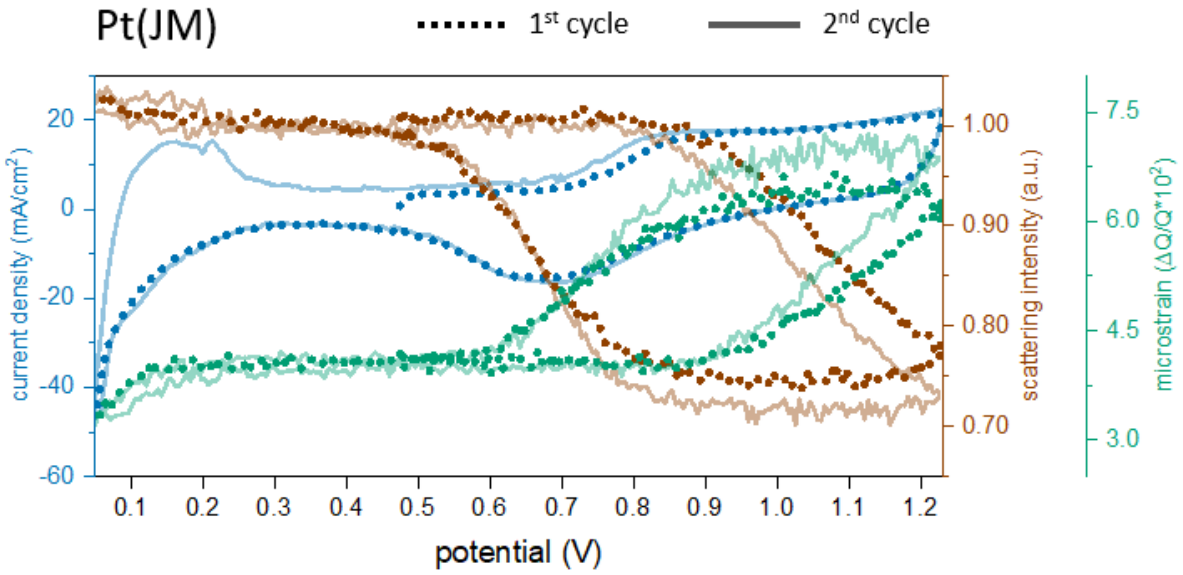

Figure S2: Differences between the 1st (dotted) and 2nd (line) cycle in XRD-CV for Pt(JM), current density (blue), scattering factor (brown), and microstrain (green)

Accelerated stress tests were performed with SP240 Biologic potentiostat, flowing O_2/H_2 200/104 sccm at 80 °C, with 80% relative humidity and 0.5 bar backpressure. The total number of 10k cycles with either (0.6 to 0.95) V or (0.7 to 0.95) V were performed.

X-ray diffraction

XRD data were collected at the ID31 beamline at the European Synchrotron Radiation Facility. A Pilatus 2M CdTe detector was used at a distance of 0.95 m. The photon wavelength was 0.161 A (77.00 keV), just below the Pt K edge. The beam size was approximately 5 × 20 µm (vertical x horizontal) with a flux of 10^{13} photons/s. An exposure time was 1 s per point for AST data and 0.1 s per point for XRD-CV. No significant beam damage was detected. Raw diffraction patterns (Figure S3a) were radially integrated using PyFAI (Kieffer and Ashiotis 2014). Integrated 1D powder diffractograms were loaded into GSAS-II, and sequential Rietveld analysis was performed (Toby and Von Dreele 2013).

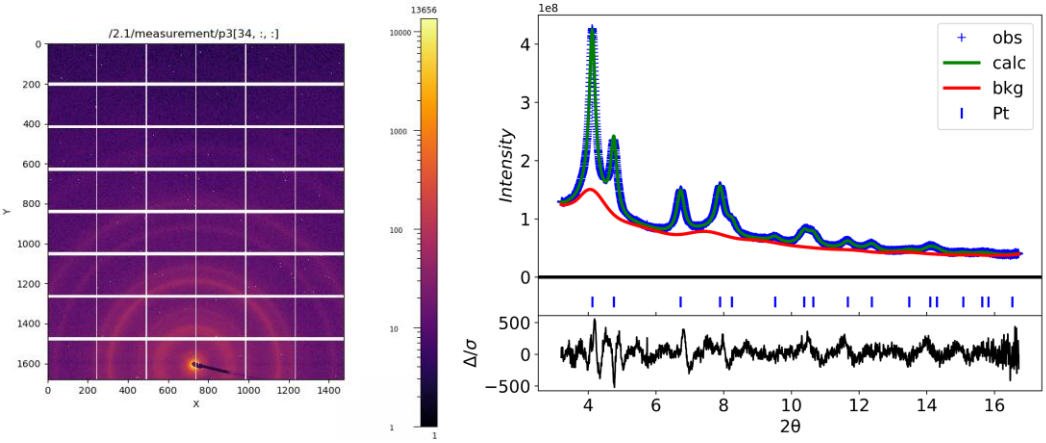

Figure S3: a) A diffraction pattern of oh-PtNiIr captured by the Pilatus 2M CdTe detector, b) Rietveld analysis of oh-PtNiIr radially integrated diffraction pattern.

Transmission electron microscopy

The measurements were conducted using a Tecnai G2 20 s-Twin microscope, equipped with a LaB6-cathode and a GATAN MS794 P CCD-detector at ZELMI Centrum, Technical

University of Berlin. TEM samples were ultrasonicated in i-PrOH and drop-dried on copper grids.

Inductively Coupled Plasma Optical Emission Spectrometry

ICP-OES was used to determine the elemental composition of the various catalysts. Samples were prepared by dissolving 5 mg of the catalyst powder with 20 mg of $NaClO_3$ in a mixture of HCl and HNO_3 (3:1). The solutions were kept for 20 min at 180 °C using a Microwave Discover SP-D (CEM Corporation). The heating ramp was 15 °C/min. Subsequently, the solutions were diluted with Milli-Q® water, filtered, and brought to a known volume. To calculate the concentration of the different solutions, five standards of Pt, Ni, and Ir were prepared with concentrations of (1, 2, 7, 12, 20) mg/L for each element.

Energy-dispersive X-ray

EDX, used for additional determination of elemental composition within samples, was carried out using XFlash 6|10 spectrometer (Bruker) installed within the MIRA III scanning electron microscope (Tescan). The primary electron beam energy was 20 keV. The area for spectra acquisition was 150um x 150um. Additionally, an area of 1000um x 1000um was used to rule out local inhomogeneities. PB-ZAF approach was used for peak deconvolution.

Author Information and Notes

Corresponding Authors

Jakub Drnec - ESRF - The European Synchrotron, ID31 Beamline, Grenoble, France

Authors

Michal Ronovsky - ESRF - The European Synchrotron, ID31 Beamline, Grenoble, France; https://orcid.org/0000-0002-8702-6056
Lujin Pan - Electrochemical Energy, Catalysis and Material Science Laboratory, Department of Chemistry, Technical University Berlin, Berlin, Germany
Malte Klingenhof - Electrochemical Energy, Catalysis and Material Science Laboratory, Department of Chemistry, Technical University Berlin, Berlin, Germany
Isaac Martens - ESRF - The European Synchrotron, ID31 Beamline, Grenoble, France
Raphael Chattot - ESRF - The European Synchrotron, ID31 Beamline, Grenoble, France
Lukas Fusek - Charles University, Faculty of Mathematics and Physics, Department of Surface and Plasma Science, V Holešovičkách 2, 180 00, Prague 8, Czech Republic
Peter Kus - Charles University, Faculty of Mathematics and Physics, Department of Surface and Plasma Science, V Holešovičkách 2, 180 00, Prague 8, Czech Republic
Marta Mirolo - ESRF - The European Synchrotron, ID31 Beamline, Grenoble, France
Fabio Dionigi - Electrochemical Energy, Catalysis and Material Science Laboratory, Department of Chemistry, Technical University Berlin, Berlin, Germany
Harriet Burdett - Johnson Matthey Technology Centre, Blount’s Court, Sonning Common, Reading RG4 9NH, U.K.
Jonathan Sharman - Johnson Matthey Technology Centre, Blount’s Court, Sonning Common, Reading RG4 9NH, U.K.
Peter Strasser - Electrochemical Energy, Catalysis and Material Science Laboratory, Department of Chemistry, Technical University Berlin, Berlin, Germany
Alex Martinez Bonastre - Johnson Matthey Technology Centre, Blount’s Court, Sonning Common, Reading RG4 9NH, U.K.

Notes

The authors declare no competing financial interest.

Acknowledgments

This project has received funding from the European Union's Horizon 2020 research and innovation program under the Marie Skłodowska-Curie grant agreement No 847439.

References

Ahluwalia, Rajesh K., Dionissios D. Papadias, Nancy N. Kariuki, Jui-Kun Peng, Xiaoping Wang, Yifen Tsai, Donald G. Graczyk, and Deborah J. Myers. 2018. "Potential Dependence of Pt and Co Dissolution from Platinum-Cobalt Alloy PEFC Catalysts Using Time-Resolved Measurements." *Journal of the Electrochemical Society* 165 (6): F3024–35.

Asset, Tristan, Raphaël Chattot, Marie Fontana, Benjamin Mercier-Guyon, Nathalie Job, Laetitia Dubau, and Frédéric Maillard. 2018. "A Review on Recent Developments and Prospects for the Oxygen Reduction Reaction on Hollow Pt-Alloy Nanoparticles." *Chemphyschem: A European Journal of Chemical Physics and Physical Chemistry* 19 (13): 1552–67.

Bi, Wu, Gary E. Gray, and Thomas F. Fuller. 2007. "PEM Fuel Cell Pt/C Dissolution and Deposition in Nafion Electrolyte." *Electrochemical and Solid-State Letters* 10 (5): B101.

Chattot, Raphaël, Pierre Bordet, Isaac Martens, Jakub Drnec, Laetitia Dubau, and Frédéric Maillard. 2020. "Building Practical Descriptors for Defect Engineering of Electrocatalytic Materials." *ACS Catalysis* 10 (16): 9046–56.

Chattot, Raphaël, Olivier Le Bacq, Vera Beermann, Stefanie Kühl, Juan Herranz, Sebastian Henning, Laura Kühn, et al. 2018. "Surface Distortion as a Unifying Concept and Descriptor in Oxygen Reduction Reaction Electrocatalysis." *Nature Materials* 17 (9): 827–33.

Chattot, Raphaël, Isaac Martens, Marta Mirolo, Michal Ronovsky, Florian Russello, Helena Isern, Guillaume Braesch, et al. 2021. "Electrochemical Strain Dynamics in Noble Metal Nanocatalysts." *Journal of the American Chemical Society* 143 (41): 17068–78.

Chattot, Raphaël, Camille Roiron, Kavita Kumar, Vincent Martin, Carlos Augusto Campos Roldan, Marta Mirolo, Isaac Martens, et al. 2022. "Break-In Bad: On the Conditioning of Fuel Cell Nanoalloy Catalysts." *ACS Catalysis*, December, 15675–85.

Cherevko, Serhiy. 2018. "Stability and Dissolution of Electrocatalysts: Building the Bridge between Model and 'real World' Systems." *Current Opinion in Electrochemistry* 8 (March): 118–25.

Cherevko, Serhiy, Gareth P. Keeley, Simon Geiger, Aleksandar R. Zeradjanin, Nejc Hodnik, Nadiia Kulyk, and Karl J. J. Mayrhofer. 2015. "Dissolution of Platinum in the Operational Range of Fuel Cells." *ChemElectroChem* 2 (10): 1471–78.

Cui, Chunhua, Lin Gan, Hui-Hui Li, Shu-Hong Yu, Marc Heggen, and Peter Strasser. 2012. "Octahedral PtNi Nanoparticle Catalysts: Exceptional Oxygen Reduction Activity by Tuning the Alloy Particle Surface Composition." *Nano Letters* 12 (11): 5885–89.

Denton, A. R., and N. W. Ashcroft. 1991. "Vegard's Law." *Physical Review. A* 43 (6): 3161–64.

Dionigi, F., C. Cesar Weber, M. Primbs, M. Gocyla, A. Martinez Bonastre, C. Spöri, H. Schmies, et al. 2019. "Controlling Near-Surface Ni Composition in Octahedral PtNi(Mo) Nanoparticles by Mo Doping for a Highly Active Oxygen Reduction Reaction Catalyst." *Nano Letters* 19 (10): 6876–85.

Drnec, Jakub, Martin Ruge, Finn Reikowski, Björn Rahn, Francesco Carlà, Roberto Felici, Jochim Stettner, Olaf M. Magnussen, and David A. Harrington. 2017. "Initial Stages of Pt(111) Electrooxidation: Dynamic and Structural Studies by Surface X-Ray Diffraction." *Electrochimica Acta* 224 (January): 220–27.

Dubau, Laetitia, Tristan Asset, Raphaël Chattot, Céline Bonnaud, Victor Vanpeene, Jaysen Nelayah, and Frédéric Maillard. 2015. "Tuning the Performance and the Stability of Porous Hollow PtNi/C Nanostructures for the Oxygen Reduction Reaction." *ACS Catalysis* 5 (9): 5333–41.

Đukić, Tina, Leonard Jean Moriau, Luka Pavko, Mitja Kostelec, Martin Prokop, Francisco Ruiz-Zepeda, Martin Šala, Goran Dražić, Matija Gatalo, and Nejc Hodnik. 2022. "Understanding the Crucial Significance of the Temperature and Potential Window on the Stability of Carbon Supported Pt-Alloy Nanoparticles as Oxygen Reduction Reaction Electrocatalysts." *ACS Catalysis* 12 (1): 101–15.

Ehelebe, Konrad, Julius Knöppel, Markus Bierling, Britta Mayerhöfer, Thomas Böhm, Nadiia Kulyk, Simon Thiele, Karl J. J. Mayrhofer, and Serhiy Cherevko. 2021. "Platinum Dissolution in Realistic Fuel Cell Catalyst Layers." *Angewandte Chemie* 60 (16): 8882–88.

Fuchs, Timo, Jakub Drnec, Federico Calle-Vallejo, Natalie Stubb, Daniel J. S. Sandbeck, Martin Ruge, Serhiy Cherevko, David A. Harrington, and Olaf M. Magnussen. 2020. “Structure Dependency of the Atomic-Scale Mechanisms of Platinum Electro-Oxidation and Dissolution.” *Nature Catalysis* 3 (9): 754–61.

Gasteiger, Hubert A., Shyam S. Kocha, Bhaskar Sompalli, and Frederick T. Wagner. 2005. “Activity Benchmarks and Requirements for Pt, Pt-Alloy, and Non-Pt Oxygen Reduction Catalysts for PEMFCs.” *Applied Catalysis. B, Environmental* 56 (1-2): 9–35.

Gatalo, Matija, Alejandro Martinez Bonastre, Léonard Jean Moriau, Harriet Burdett, Francisco Ruiz-Zepeda, Edwin Hughes, Adam Hodgkinson, et al. 2022. “Importance of Chemical Activation and the Effect of Low Operation Voltage on the Performance of Pt-Alloy Fuel Cell Electrocatalysts.” *ACS Applied Energy Materials* 5 (7): 8862–77.

Hammer, B., and J. K. Nørskov. 2000. “Theoretical Surface Science and Catalysis—calculations and Concepts.” In *Advances in Catalysis*, 45:71–129. Academic Press.

Huang, Yan, Junliang Zhang, Anusorn Kongkanand, Frederick T. Wagner, James C. M. Li, and Jacob Jorné. 2014. “Transient Platinum Oxide Formation and Oxygen Reduction on Carbon-Supported Platinum and Platinum-Cobalt Alloy Electrocatalysts.” *Journal of the Electrochemical Society* 161 (1): F10–15.

Imai, Hideto, Koichi Izumi, Masashi Matsumoto, Yoshimi Kubo, Kazuo Kato, and Yasuhiko Imai. 2009. “In Situ and Real-Time Monitoring of Oxide Growth in a Few Monolayers at Surfaces of Platinum Nanoparticles in Aqueous Media.” *Journal of the American Chemical Society* 131 (17): 6293–6300.

Jacobse, Leon, Marcel J. Rost, and Marc T. M. Koper. 2019. “Atomic-Scale Identification of the Electrochemical Roughening of Platinum.” *ACS Central Science* 5 (12): 1920–28.

Janik, Michael J., Ian T. McCrum, and Marc T. M. Koper. 2018. “On the Presence of Surface Bound Hydroxyl Species on Polycrystalline Pt Electrodes in the ‘hydrogen Potential Region’ (0–0.4 V-RHE).” *Journal of Catalysis* 367 (November): 332–37.

Kawaguchi, Tomoya, Vladimir Komanicky, Vitalii Latyshev, Wonsuk Cha, Evan R. Maxey, Ross Harder, Tetsu Ichitsubo, and Hoydoo You. 2021. “Electrochemically Induced Strain Evolution in Pt-Ni Alloy Nanoparticles Observed by Bragg Coherent Diffraction Imaging.” *Nano Letters* 21 (14): 5945–51.

Khedekar, Kaustubh, Morteza Rezaei Talarposhti, Münir M. Besli, Saravanan Kuppan, Andrea Perego, Yechuan Chen, Michael Metzger, et al. 2021. “Probing Heterogeneous Degradation of Catalyst in PEM Fuel Cells under Realistic Automotive Conditions with Multi- modal Techniques.” *Advanced Energy Materials* 11 (35): 2101794.

Kieffer, Jérôme, and Giannis Ashiotis. 2014. “PyFAI: A Python Library for High Performance Azimuthal Integration on GPU.” https://doi.org/10.48550/ARXIV.1412.6367.

Kim, Cheonghee, Fabio Dionigi, Vera Beermann, Xingli Wang, Tim Möller, and Peter Strasser. 2019. “Alloy Nanocatalysts for the Electrochemical Oxygen Reduction (ORR) and the Direct Electrochemical Carbon Dioxide Reduction Reaction (CO RR).” *Advanced Materials* 31 (31): e1805617.

Kitchin, J. R., J. K. Nørskov, M. A. Barteau, and J. G. Chen. 2004. “Role of Strain and Ligand Effects in the Modification of the Electronic and Chemical Properties of Bimetallic Surfaces.” *Physical Review Letters* 93 (15): 156801.

Kneer, Alexander, Nadja Wagner, Christian Sadeler, Anne-Christine Scherzer, and Dietmar Gerteisen. 2018. “Effect of Dwell Time and Scan Rate during Voltage Cycling on Catalyst Degradation in PEM Fuel Cells.” *Journal of the Electrochemical Society* 165 (10): F805–12.

Kongkanand, Anusorn, and Mark F. Mathias. 2016. “The Priority and Challenge of High-Power Performance of Low-Platinum Proton-Exchange Membrane Fuel Cells.” *Journal of Physical Chemistry Letters* 7 (7): 1127–37.

Kongkanand, Anusorn, and Joseph M. Ziegelbauer. 2012. “Surface Platinum Electrooxidation in the Presence of Oxygen.” *The Journal of Physical Chemistry. C, Nanomaterials and Interfaces* 116 (5): 3684–93.

Lee, H. C., B. M. Kim, C. K. Jeong, R. Toyoshima, H. Kondoh, T. Shimada, K. Mase, et al. 2016. “Surface Segregation and Oxidation of Pt3Ni(111) Alloys under Oxygen Environment.” *Catalysis Today* 260 (February): 3–7.

Leineweber, Andreas. 2011. “Understanding Anisotropic Microstrain Broadening in Rietveld Refinement.” *Zeitschrift Fur Kristallographie* 226 (12): 905–23.

Li, Kan, Xingxing Li, Hongwen Huang, Laihao Luo, Xu Li, Xupeng Yan, Chao Ma, Rui Si, Jinlong Yang, and Jie Zeng. 2018. “One-Nanometer-Thick PtNiRh Trimetallic Nanowires with Enhanced Oxygen Reduction Electrocatalysis in Acid Media: Integrating Multiple Advantages into One Catalyst.” *Journal of the American Chemical Society* 140 (47): 16159–67.

Lin, Rui, Lu Che, Dandan Shen, and Xin Cai. 2020. “High Durability of Pt-Ni-Ir/C Ternary Catalyst of PEMFC by Stepwise Reduction Synthesis.” *Electrochimica Acta* 330 (135251): 135251.

Lopes, Pietro P., Dusan Tripkovic, Pedro F. B. D. Martins, Dusan Strmcnik, Edson A. Ticianelli, Vojislav R. Stamenkovic, and Nenad M. Markovic. 2018. “Dynamics of Electrochemical Pt Dissolution at Atomic and Molecular Levels.” *Journal of Electroanalytical Chemistry* 819 (June): 123–29.

Ly, Alvin, Tristan Asset, and Plamen Atanassov. 2020. “Integrating Nanostructured Pt-Based Electrocatalysts in Proton Exchange Membrane Fuel Cells.” *Journal of Power Sources* 478 (228516): 228516.

Marković, N. M., T. J. Schmidt, V. Stamenković, and P. N. Ross. 2001. “Oxygen Reduction Reaction on Pt and Pt Bimetallic Surfaces: A Selective Review.” *Fuel Cells* 1 (2): 105–16.

Martens, Isaac, Raphaël Chattot, and Jakub Drnec. 2022. “Decoupling Catalyst Aggregation, Ripening, and Coalescence Processes inside Operating Fuel Cells.” *Journal of Power Sources* 521 (230851): 230851.

Martens, Isaac, Raphael Chattot, Miika Rasola, Maria Valeria Blanco, Veijo Honkimäki, Dan Bizzotto, David P. Wilkinson, and Jakub Drnec. 2019. “Probing the Dynamics of Platinum Surface Oxides in Fuel Cell Catalyst Layers Using in Situ X-Ray Diffraction.” *ACS Applied Energy Materials* 2 (11): 7772–80.

Martens, Isaac, Raphael Chattot, Tim Wiegmann, Timo Fuchs, Olaf M. Magnussen, Laetitia Dubau, Frederic Maillard, and Jakub Drnec. 2021. “Towards Comprehensive Understanding of Proton-Exchange Membrane Fuel Cells Using High Energy X-Rays.” *Journal of Physics: Energy* 3 (3): 031003.

Martens, Isaac, Antonis Vamvakeros, Raphael Chattot, Maria V. Blanco, Miika Rasola, Janne Pusa, Simon D. M. Jacques, et al. 2019. “X-Ray Transparent Proton-Exchange Membrane Fuel Cell Design for in Situ Wide and Small Angle Scattering Tomography.” *Journal of Power Sources* 437 (226906): 226906.

Myers, Deborah J., Xiaoping Wang, Matt C. Smith, and Karren L. More. 2018. “Potentiostatic and Potential Cycling Dissolution of Polycrystalline Platinum and Platinum Nano-Particle Fuel Cell Catalysts.” *Journal of the Electrochemical Society* 165 (6): F3178–90.

Nagy, Zoltán, and Hoydoo You. 2002. “Applications of Surface X-Ray Scattering to Electrochemistry Problems.” *Electrochimica Acta* 47 (19): 3037–55.

Nørskov, Jens K., Frank Abild-Pedersen, Felix Studt, and Thomas Bligaard. 2011. “Density Functional Theory in Surface Chemistry and Catalysis.” *Proceedings of the National Academy of Sciences of the United States of America* 108 (3): 937–43.

Nørskov, J. K., T. Bligaard, J. Rossmeisl, and C. H. Christensen. 2009. “Towards the Computational Design of Solid Catalysts.” *Nature Chemistry* 1 (1): 37–46.

O’Hayre, Ryan, and Fritz B. Prinz. 2004. “The Air/platinum/nafion Triple-Phase Boundary: Characteristics, Scaling, and Implications for Fuel Cells.” *Journal of the Electrochemical Society* 151 (5): A756.

Okonkwo, Paul C., Oladeji O. Ige, El Manaa Barhoumi, Paul C. Uzoma, Wilfred Emori, Abdelbaki Benamor, and Aboubakr M. Abdullah. 2021. “Platinum Degradation Mechanisms in Proton Exchange Membrane Fuel Cell (PEMFC) System: A Review.” *International Journal of Hydrogen Energy* 46 (29): 15850–65.

Pan, Lujin, Sebastian Ott, Fabio Dionigi, and Peter Strasser. 2019. “Current Challenges Related to the Deployment of Shape-Controlled Pt Alloy Oxygen Reduction Reaction Nanocatalysts into Low Pt-Loaded Cathode Layers of Proton Exchange Membrane Fuel Cells.” *Current Opinion in Electrochemistry* 18 (December): 61–71.

Politano, A., M. Caputo, A. Goldoni, P. Torelli, and G. Chiarello. 2013. “Segregation and Selective Oxidation of Ni Atoms in Pt3Ni(111) in a Low-Pressure Oxygen Environment.” *Journal of Physical Chemistry C* 117 (51): 27007–11.

Politano, Antonio, and Gennaro Chiarello. 2016. “Unveiling the Oxidation Processes of Pt3Ni(1 1 1) by Real-Time Surface Core-Level Spectroscopy.” *ChemCatChem* 8 (4): 713–18.

Prokop, Martin, Monika Drakselova, and Karel Bouzek. 2020. “Review of the Experimental Study and Prediction of Pt-Based Catalyst Degradation during PEM Fuel Cell Operation.” *Current Opinion in Electrochemistry* 20 (April): 20–27.

Ruge, Martin, Jakub Drnec, Björn Rahn, Finn Reikowski, David A. Harrington, Francesco Carlà, Roberto Felici, Jochim Stettner, and Olaf M. Magnussen. 2017a. “Electrochemical Oxidation of Smooth and Nanoscale Rough pt(111): An in Situ Surface X-Ray Scattering Study.” *Journal of the Electrochemical Society* 164 (9): H608–14.

———. 2017b. “Structural Reorganization of Pt(111) Electrodes by Electrochemical Oxidation and Reduction.” *Journal of the American Chemical Society* 139 (12): 4532–39.

Sandbeck, Daniel J. S., Niklas Mørch Secher, Florian D. Speck, Jakob Ejler Sørensen, Jakob Kibsgaard, Ib Chorkendorff, and Serhiy Cherevko. 2020. “Particle Size Effect on Platinum Dissolution: Considerations for Accelerated Stability Testing of Fuel Cell Catalysts.” *ACS Catalysis* 10 (11): 6281–90.

Sasaki, Kotaro, Minhua Shao, and Radoslav Adzic. 2009. “Dissolution and Stabilization of Platinum in Oxygen Cathodes.” In *Polymer Electrolyte Fuel Cell Durability*, 7–27. New York, NY: Springer New York.

Sharma, Raghunandan, and Shuang Ma Andersen. 2018. “Zoom in Catalyst/Ionomer Interface in Polymer Electrolyte Membrane Fuel Cell Electrodes: Impact of Catalyst/Ionomer Dispersion Media/Solvent.” *ACS Applied Materials & Interfaces* 10 (44): 38125–33.

Stamenkovic, Vojislav R., Bongjin Simon Mun, Matthias Arenz, Karl J. J. Mayrhofer, Christopher A. Lucas, Guofeng Wang, Philip N. Ross, and Nenad M. Markovic. 2007. “Trends in Electrocatalysis on Extended and Nanoscale Pt-Bimetallic Alloy Surfaces.” *Nature Materials* 6 (3): 241–47.

Toby, Brian H., and Robert B. Von Dreele. 2013. “GSAS-II: The Genesis of a Modern Open-Source All Purpose Crystallography Software Package.” *Journal of Applied Crystallography* 46 (2): 544–49.

Topalov, Angel A., Serhiy Cherevko, Aleksandar R. Zeradjanin, Josef C. Meier, Ioannis Katsounaros, and Karl J. J. Mayrhofer. 2014. “Towards a Comprehensive Understanding of Platinum Dissolution in Acidic Media.” *Chemical Science* 5 (2): 631–38.

Uchimura, Masanobu, Seiho Sugawara, Yosuke Suzuki, Jianbo Zhang, and Shyam S. Kocha. 2008. “Electrocatalyst Durability under Simulated Automotive Drive Cycles.” In *ECS Transactions*. ECS. https://doi.org/10.1149/1.2981858.

Vegard, L. 1921. “Die Konstitution der Mischkristalle und die Raumf[illegible]llung der Atome.” *European Physical Journal A: Hadrons and Nuclei* 5 (1): 17–26.

Wang, Xiaoping, Romesh Kumar, and Deborah J. Myers. 2006. “Effect of Voltage on Platinum Dissolution.” *Electrochemical and Solid-State Letters* 9 (5): A225.

Weissmüller, J., R. N. Viswanath, D. Kramer, P. Zimmer, R. Würschum, and H. Gleiter. 2003. “Charge-Induced Reversible Strain in a Metal.” *Science* 300 (5617): 312–15.

Xin, Hongliang, Aleksandra Vojvodic, Johannes Voss, Jens K. Nørskov, and Frank Abild-Pedersen. 2014. “Effects of D-Band Shape on the Surface Reactivity of Transition-Metal Alloys.” *Physical Review. B, Condensed Matter* 89 (11): 115114.

You, H., and Z. Nagy. 1994. “Oxidation-Reduction-Induced Roughening of Platinum (1 1 1) Surface.” *Physica. B, Condensed Matter* 198 (1): 187–94.

You, H., D. J. Zurawski, Z. Nagy, and R. M. Yonco. 1994. “In- situ X- ray Reflectivity Study of Incipient Oxidation of Pt(111) Surface in Electrolyte Solutions.” *The Journal of Chemical Physics* 100 (6): 4699–4702.

Zhang, Changlin, Xiaochen Shen, Yanbo Pan, and Zhenmeng Peng. 2017. “A Review of Pt-Based Electrocatalysts for Oxygen Reduction Reaction.” *Frontiers of Energy and Power Engineering in China* 11 (3): 268–85.

Zhang, Hao, Herwig Haas, Jingwei Hu, Sumit Kundu, Mike Davis, and Carmen Chuy. 2013. “The Impact of Potential Cycling on PEMFC Durability.” *Journal of the Electrochemical Society* 160 (8): F840–47.

Zhang, Jiawei, Yuliang Yuan, Lei Gao, Gangming Zeng, Mengfan Li, and Hongwen Huang. 2021. “Stabilizing Pt-Based Electrocatalysts for Oxygen Reduction Reaction: Fundamental Understanding and Design Strategies.” *Advanced Materials* 33 (20): e2006494.